ACSNANO

www.acsnano.org

ARTICLE

Remanent Polarization and Strong Photoluminescence Modulation by an External Electric Field in Epitaxial $CsPbBr_3$ Nanowires

Ella Sanders,[#] Yahel Soffer,[#] Tommaso Salzillo, Maor Rosenberg, Omri Bar-Elli, Omer Yaffe, Ernesto Joselevich,* and Dan Oron*

Cite This: *ACS Nano* 2021, 15, 16130–16138

Read Online

ACCESS | Metrics & More | Article Recommendations | Supporting Information

ABSTRACT: **Metal halide perovskites (MHPs) have unique characteristics and hold great potential for next-generation optoelectronic technologies. Recently, the importance of lattice strain in MHPs has been gaining recognition as a significant optimization parameter for device performance. While the effect of strain on the fundamental properties of MHPs has been at the center of interest, its combined effect with an external electric field has been largely overlooked. Here we perform an electric-field-dependent photoluminescence study on heteroepitaxially strained surface-guided $CsPbBr_3$ nanowires. We reveal an unexpected strong linear dependence of the photoluminescence intensity on the alternating field amplitude, stemming from an induced internal dipole. Using low-frequency polarized-Raman spectroscopy, we reveal structural modifications in the nanowires under an external field, associated with the observed polarity. These results reflect the important interplay between strain and an external field in MHPs and offer opportunities for the design of MHP-based optoelectronic nanodevices.**

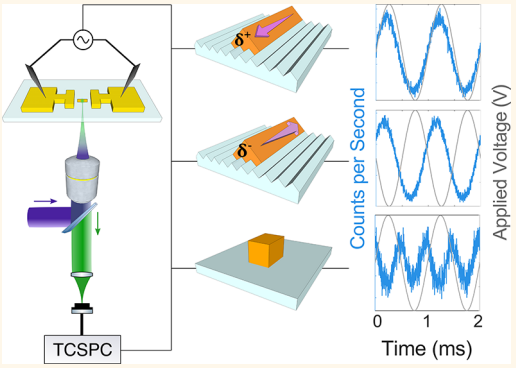

KEYWORDS: *metal halide perovskites, epitaxial strain, electro-optics, nanowires, photoluminescence*

INTRODUCTION

The promising optoelectronic properties of metal halide perovskites (MHPs) have led to extensive research aiming to discover the source of their extraordinary performance and to fulfill their potential as building blocks for optoelectronic devices, including photovoltaics, light sources, and detectors. As semiconductors, MHPs' properties may be significantly influenced by the presence of lattice strain, especially in light of their mechanically soft nature.[1] While mismanaged strain can often lead to defect formation and material degradation, strain engineering can introduce beneficial effects.[2,3] One of the most common techniques in use is heteroepitaxial strain engineering, where the strain is created due to a lattice mismatch between a crystalline substrate and the desired epilayer. While this technique has evolved as a powerful tool in MHPs,[2] it is currently limited to the case of low lattice mismatch with the substrate, often not available when designing efficient devices. Although the influence of strain on the intrinsic properties of MHPs is gaining interest, the effect of an applied electric field (E-field) on a strained system has been largely overlooked. This is despite the fact that external E-fields are commonly applied in optoelectronics, and their effect on the properties of strained MHPs is of significant importance.[4]

In order to obtain a clear understanding of the combined effect of strain and applied E-field on MHPs, we chose to focus on heteroepitaxial surface-guided $CsPbBr_3$ nanowires grown on sapphire, utilizing them as a simple quasi one-dimensional model system. We have previously reported the growth of these nanowires, forming horizontal arrays that follow the symmetry of the sapphire substrate.[5] We have shown the nanowires to have a size-dependent bandgap modulation, which was attributed to large lattice distortions arising from a combination of the heteroepitaxial mismatch and the

Received: June 9, 2021
Accepted: September 15, 2021
Published: September 21, 2021

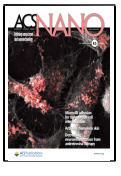

https://doi.org/10.1021/acsnano.1c04905
ACS Nano 2021, 15, 16130–16138

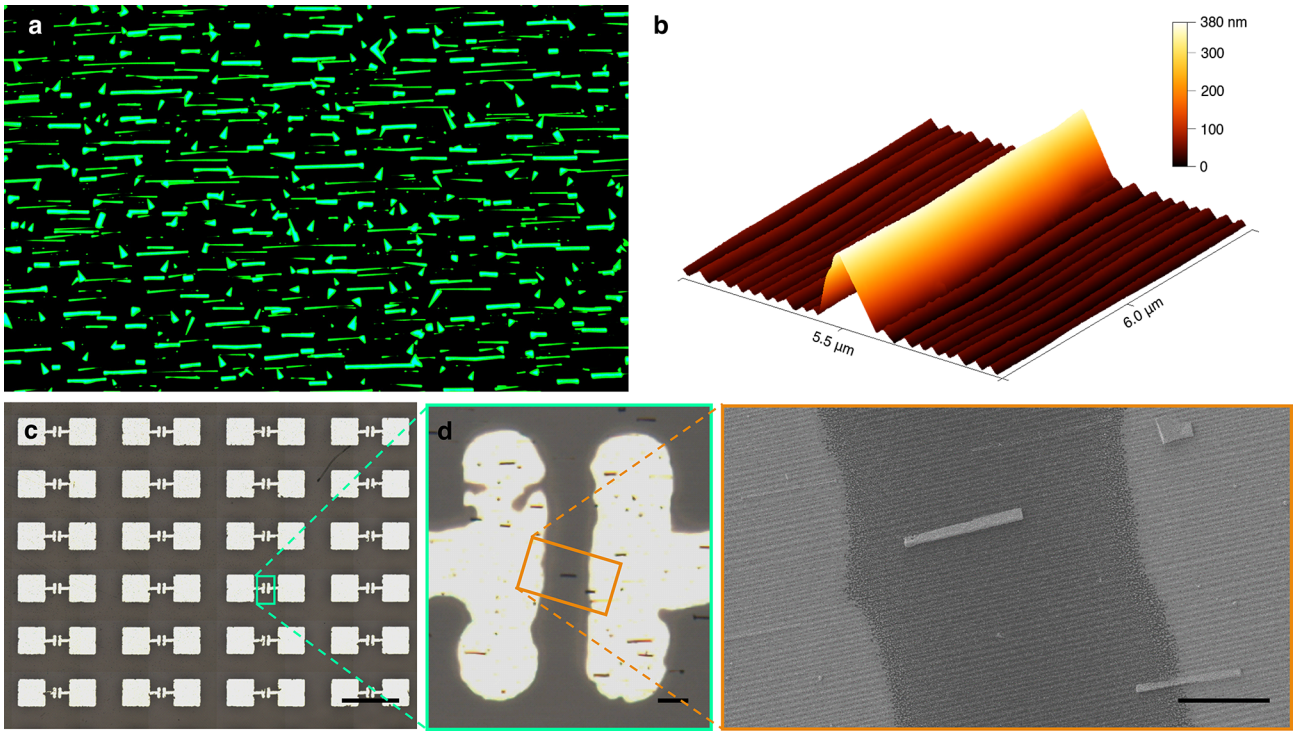

Figure 1. Surface-guided $CsPbBr_3$ nanowires on annealed M-plane sapphire. (a) Optical microscope image of an array of surface-guided nanowires emitting green luminescence under excitation with a wide-spectrum UV light. Scale bar: 20 μm. (b) Atomic force microscope (AFM) image, presenting a typical nanowire with the characteristic triangular cross-section and the nanogrooves on the surface of the sapphire. (c) Optical microscope image of an array of parallely fabricated microdevices. Scale bar: 500 μm. (d) Optical microscope image of a typical device (zoom-in on the green rectangle in (c)). Scale bar: 10 μm. (e) Scanning electron microscope (SEM) image of a single nanowire between two electrodes (zoom-in on the orange rectangle in (d)). Scale bar: 5 μm.

significant difference between the thermal expansion coefficients of $CsPbBr_3$ and sapphire.[6]

Here, we perform an E-field-dependent photoluminescence (PL) study on single heteroepitaxially strained surface-guided $CsPbBr_3$ nanowires on sapphire. We reveal an intriguing linear dependence of the PL intensity on the applied alternating external E-field, reaching a considerable modulation depth of up to 40% in the PL, accompanied by very slow carrier dynamics, on the time scale of milliseconds. This asymmetric response, upon which the PL increases in one orientation of the E-field and decreases in the other, is surprising since these nanowires are considered to possess an averaged centrosymmetric structure.[6] We show that it stems from a permanent dipole generated in the nanowires, where in the majority of the examined nanowires, the direction of the induced dipole was determined by the initial direction of the applied field. This internal dipole could not be reversed on a time scale of several weeks, even when applying opposite DC fields of a higher magnitude. We establish a clear link between the heteroepitaxial strain and the nanowires' induced polarity *via* comparison with $CsPbBr_3$ crystals grown using alternative methods. Finally, by using polarization-orientation (PO) Raman spectroscopy, we confirm that the nanowires undergo a structural change under an applied E-field, associated with the observed polarity. Our findings unambiguously indicate the significant impact of an external E-field on the structure and optoelectronic properties of a heteroepitaxially strained system of $CsPbBr_3$, having potential implications on the performance of MHP-based optoelectronic devices and potentially enabling external control over the luminescence of MHPs.

RESULTS AND DISCUSSION

Surface-Guided $CsPbBr_3$ Nanowires. Surface-guided $CsPbBr_3$ nanowires were grown on sapphire in a vapor-phase method.[7] We focused on annealed M-plane sapphire, where nanogrooves on the surface direct the growth in two opposite directions, creating an array of horizontally parallel nanowires (Figure 1a,b).[8,9] This graphoepitaxial growth, guided by nanofeatures on the surface, forces the nanowires to epitaxially accommodate to both exposed facets of the nanogroove.[10] This introduces strain in the $CsPbBr_3$ crystal lattice, which is highest at the interface with the sapphire and gradually decreases toward the top of the nanowire.[6] The measured nanowires exhibit the expected stoichiometry of $CsPbBr_3$ (Figure S1) and are up to 8 μm in length and a few hundreds of nanometers in height. They are randomly self-nucleated, possess a triangular cross-section (Figure 1b), and all grow along the (001) growth direction.[5] In order to investigate the effect of an external E-field on the properties of the strained nanowires, we fabricated an array of two-electrode devices, such that the nanowire's long axis is parallel to the E-field lines (Figure 1c–e). We prevent electrochemical interactions and charge injection into the nanowires by measuring in a contactless configuration, where there is no current flow between the electrodes and the nanowires.

E-Field-Dependent PL Intensity of Surface-Guided $CsPbBr_3$ Nanowires. The E-field-dependent PL spectroscopy studies on single nanowires were done in an epifluorescence microscope configuration, collecting light emitted from a single nanowire (Figure 2a, see Methods). While the nanowire is excited with a 405 nm continuous wave (CW) laser, we apply

https://doi.org/10.1021/acsnano.1c04905
ACS Nano 2021, 15, 16130–16138

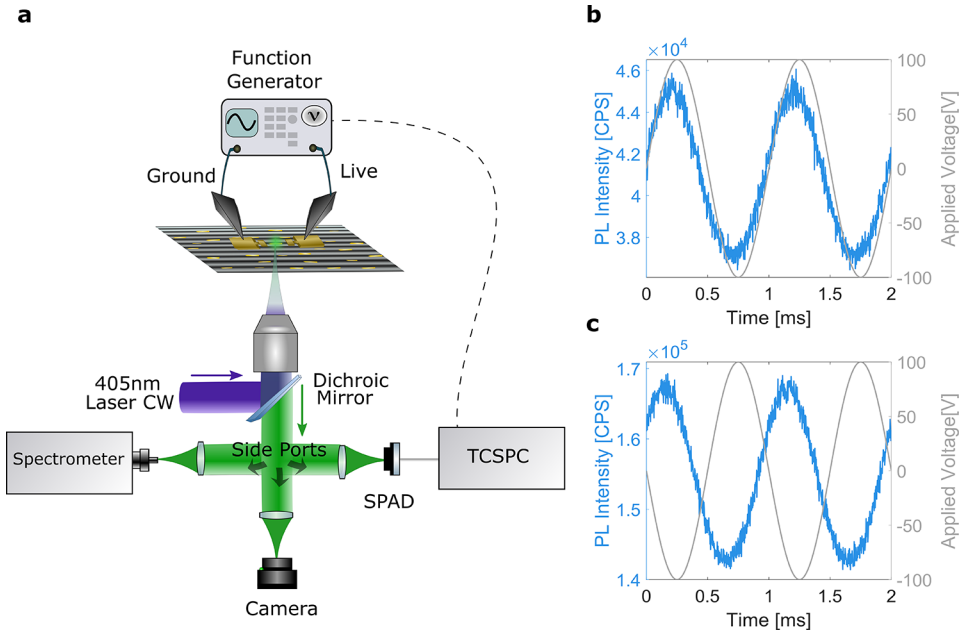

Figure 2. E-field-dependent PL intensity of surface-guided $CsPbBr_3$ nanowires. (a) Scheme of the optoelectronic setup. Single nanowires are illuminated through an inverted optical microscope with a CW 405 nm laser, while an AC voltage is applied to the surrounding pair of electrodes. The epi-detected signal is projected into one of three ports. One port is coupled into a spectrometer, the second is imaged onto an EMCCD camera for orientation on the sample, and the third port is coupled to a SPAD, which is connected to a time-correlated single photon counting (TCSPC) system (see Methods). (b and c) Representative PL intensity responses of two oppositely polarized surface-guided $CsPbBr_3$ nanowires to an oscillating sinewave E-field (b) in-phase with respect to a sine E-field in the lab frame and (c) antiphase with respect to a π-shifted sine E-field in the lab frame.

an oscillating E-field (10^6–10^7 V/m, typically at 1 kHz) to the surrounding pair of electrodes using microprobes. The PL is directed toward a single-photon avalanche photodiode (SPAD) connected to a photon-counting and timing system, from which we retrieve the arrival time of each emitted photon and correlate it with the oscillation of the E-field. Finally, we obtain the averaged PL intensity time trace with respect to the AC cycle. When subjected to an AC field with a sine waveform, the nanowires exhibit a linear, asymmetric PL response with respect to the modulating E-field (Figure 2b). This linear response is surprising for centrosymmetric crystals, which are expected to exhibit a lowest order quadratic response due to symmetry requirements.[11] Such a linear response is characteristic of an asymmetric (polar) system having an internal field. In addition to the intriguing asymmetry, we found that for a significant majority of the nanowires, the initial direction of the field (with respect to the lab frame) set the direction in which the PL increases. That is, PL modulation can be in-phase (for sinewave $V_{initial} > 0$, Figure 2b) or antiphase (for π-shifted sinewave $V_{initial} < 0$, Figure 2c) with the oscillating field, which appears to indicate a rapidly formed internal field in the nanowires, opposing the direction of the very initial external E-field applied. Furthermore, once the response direction is set, it cannot be flipped (on a measured time scale of several weeks), even when applying opposite DC fields of a higher magnitude (up to 2×10^7 V/m), meaning the system does not behave as a ferroelectric,[12] but rather resembles an electret,[13] a material exhibiting a dynamically stable electric dipole.[14] We note that more than 80% of the 54 measured nanowires showed PL modulation above the noise level, all responding asymmetrically, out of which about 70% followed the direction of the initial external field. Notably, it seems that the details of the synthetic conditions play an important role in determining whether the nanowire's dipole is set externally or rather set upon its formation, since in some batches of nanowires the orientation of the apparent polarity was random, whereas in others a large fraction of the nanowires seemed to follow the initial E-field.

An asymmetric E-field-modulated PL intensity in the millisecond time scale was reported before on $MAPbBr_3$ nanocrystals. However, that work exhibited both linear and nonlinear oscillatory responses of the PL intensity to the E-field (up to ~10^7 V/m at 10 Hz), which were ascribed primarily to the methylammonium cation reorientation dynamics.[15] This explanation does not apply to the inorganic $CsPbBr_3$, meaning the asymmetric PL response in the nanowires stems from a different mechanism. In order to check for a Stark-effect-related change in PL intensity, we measured PL spectra with and without applying an E-field. No apparent change was observed in the band-edge emission and spectral width for DC fields of 10^6 V/m (Figure S2), which is reasonable, as significant Stark shifts typically require stronger fields (~10^8 V/m).[16] Ion migration was linked before with PL enhancement in $CsPbBr_3$ nanocrystals under bias.[17] However, this cannot be the cause for the PL switching in our case, since the asymmetric PL response is irreversible, and the frequency range is higher (Figure 2b,c and Figure S5a) than the reported response time of ion migration in MHPs.[18]

Large Modulation Depth and Slow Carrier Dynamics under an E-Field. Close examination of the nanowires' asymmetric PL intensity response to the E-field (Figure 2b,c) reveals an apparent phase shift between the applied AC and the resultant PL intensity modulation, where the E-field modulation slightly trails the PL modulation. This indicates a transient behavior of the charge carrier recombination, which can be elucidated by looking at the response to an abrupt

https://doi.org/10.1021/acsnano.1c04905
ACS Nano 2021, 15, 16130–16138

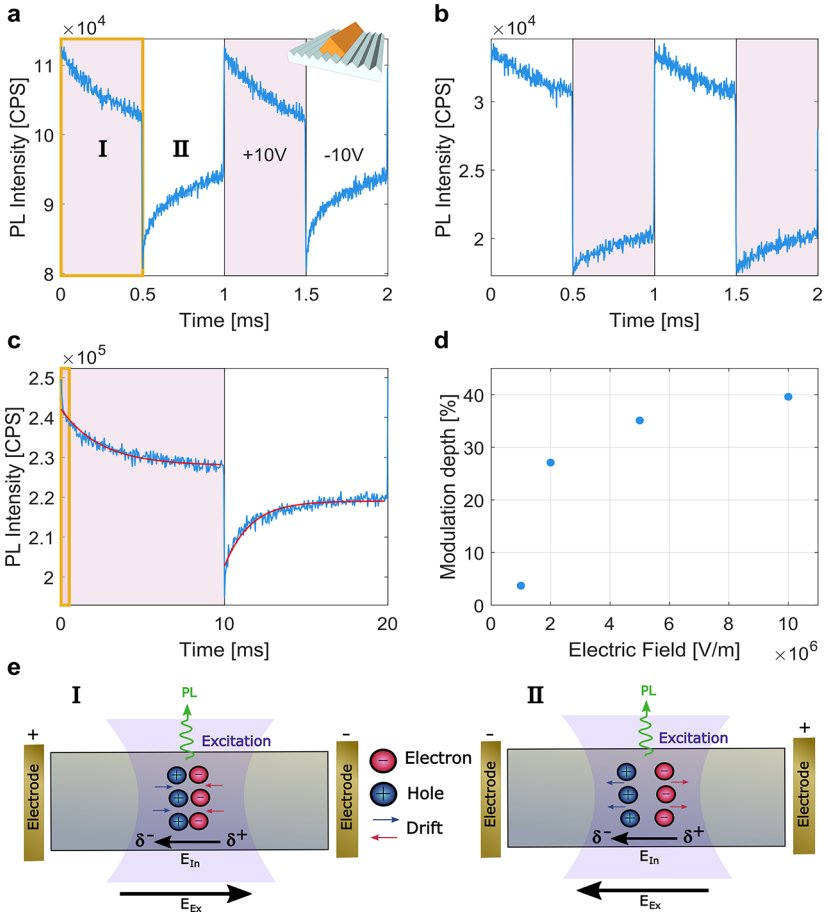

Figure 3. Slow charge carrier dynamics in surface-guided $CsPbBr_3$ nanowires. (a and b) Representative PL modulation responses of two oppositely polarized surface-guided $CsPbBr_3$ nanowires grown on an annealed M-plane as a response to an applied 10 V square wave at 1 kHz. (a) In-phase response (15% modulation depth) and (b) antiphase response (33% modulation depth) with respect to the lab frame. Inset: Scheme of a $CsPbBr_3$ surface-guided nanowire grown on annealed M-plane sapphire. (c) Typical PL modulation of the nanowires as a response to a 10 V square wave at 50 Hz (same nanowire as shown in (a)). The yellow rectangles indicate the same time scale, emphasizing the slow dynamics. The two red plots are fits to the phenomenological model (see SI section 3), which describes the radiative recombination rates for the two applied field directions. In the left half (purple area) the PL decay is fitted to $A^2e^{-2t/\tau} + 2ACe^{-t/\tau} + C^2$, where $\tau = 2.48$ ms. In the right half (white area) the PL rise is fitted to $A^2e^{-2t/\tau} - 2ACe^{-t/\tau} + C^2$, where $\tau = 1.57$ ms. (d) Typical dependency of the PL modulation depth on the external applied field using a square wave at 10 Hz, exhibiting saturation at $\sim 10^7$ V/m. (e) Scheme of the charge carrier dynamics inside the nanowires in the two states of the external E-field alignment with the internal dipole ((I) and (II), also marked in (a)). In all plots, the purple areas refer to 10 V and the white area refers to −10 V according to the lab frame, as depicted in (a).

change in the E-field. Indeed, application of a square wave E-field at 1 kHz revealed a time-dependent PL intensity response (Figure 3a,b), with a characteristic time scale that seems to be longer than the field modulation period. When measuring at a lower frequency of 50 Hz (Figure 3c), a slow decay (or rise) of several milliseconds becomes apparent. Note that the surface-guided nanowires' dimensions are orders of magnitude larger than the $CsPbBr_3$ Bohr radius of the exciton (7 nm),[19] meaning they do not fall into the quantum confinement regime, and as such, the carrier dynamics are dominated by those of free charge carriers.[20] The experimental findings can be interpreted as follows: Due to an internal dipole formed by the initial E-field, the carriers' separation in the nanowire is unidirectional to begin with, and the application of a modulating E-field alternates the spatial overlap of the carriers (both electrons and holes) depending on the E-field direction. This electrostatic maneuvering provides an indirect control over the emission rate, allowing charge storage in a single nanowire. Assuming the nonradiative decay channels are not modulated by the E-field, a significant change in the apparent quantum yield (QY) arises, reaching a considerable PL modulation depth of up to 40% (Figure 3d), without a significant difference between in-phase and antiphase within the statistical dispersion. Notably, similar E-field-induced PL switching was shown before for off-center heteronanostructures of different chalcogenides,[21,22] where their asymmetric structure enabled manipulation of the electron−hole spatial-overlap by an external E-field.

Figure 3a and b display representative responses of two single nanowires, one in-phase and the other antiphase with the electric square wave, respectively (with respect to the lab frame). In both cases, when the E-field is applied in the PL-enhancing direction, we observe a steep rise in PL intensity, which indicates a rapid increase in the radiative recombination rate due to the larger electron−hole wave function overlap, occurring when the external field opposes the internal field (Figure 3e(I)). This is followed by a slow decay over time that can be attributed to a gradual decrease in the number of free carriers. Conversely, when an E-field is applied in the opposite direction and coincides with the internal dipole direction, a

https://doi.org/10.1021/acsnano.1c04905
ACS Nano 2021, 15, 16130−16138

steep decrease in PL intensity is observed, indicating a much smaller overlap of electrons and holes and therefore a decrease in radiative recombination rate (Figure 3e(II)). This is followed by a slow rise in PL intensity, suggesting a gradual increase in the free carrier concentration. The origin of the slow rise (or decay), typically in the millisecond scale, is likely associated with long-lived carrier trapping. Notably, the difference in the asymptotes of the rise and decay observed for the two opposite field directions (Figure 3c) is representative of two different steady states of the charge carrier dynamics, indicating the presence of nonradiative decay channels. Phenomenologically, this behavior can be reproduced by a simple model considering a fixed nonradiative decay rate and bimolecular radiative decay which is modulated by the E-field due to charge carrier diffusion under the combined effect of the internal dipole and the external field, as detailed in the SI section 3. A fit of the PL transient to the model is shown for a typical nanowire as a red line in Figure 3c, exhibiting transients of about 2 ms (see Figure 3c caption). Interestingly, the PL modulation depth appears to saturate as the field becomes stronger (Figure 3d). This behavior does not follow the quadratic dependency expected from the Coulombic electron−hole interaction and might indicate a physical barrier the carriers encounter during transport (as will be discussed in the last section of the results), limiting their spatial separation induced by the external field.

Role of Heteroepitaxial Strain in the Formation of the Internal Field. In trying to elucidate the origin of our observations and to identify whether they stem from an intrinsic characteristic of $CsPbBr_3$ or rather are specific to the surface-guided nanowires, we measured submicron-sized $CsPbBr_3$ crystals, synthesized in solution,[23] deposited on sapphire in between electrodes of the same configuration. These crystals exhibit a quadratic PL response to the modulating field, where both directions of the field lead to attenuation of the PL intensity (Figure 4a). This is the expected response of a centrosymmetric crystal, as these single crystals were reported to be.[23] To reinforce this finding, we measured two types of colloidal $CsPbBr_3$ nanocrystals of dimensions of the order of 10 and 100 nm. Both sizes exhibited a symmetric response (Figure S5b,c), further demonstrating the expected perturbation introduced by an external modulating E-field to the charge carrier dynamics in a centrosymmetric crystal. It is also important to note the magnitude of the responses; while the surface-guided nanowires exhibit a considerable modulation depth, all solution-grown crystals present a modulation depth lower by at least an order of magnitude.

The clear and main difference between the surface-guided nanowires and the other submicron $CsPbBr_3$ crystals is the heteroepitaxial strain present in the crystal lattice of the nanowires. As mentioned above, our previous work has shown this strain to be the cause of large lattice distortions that affect the bandgap size,[6] which, in principle, can affect the structural stability and charge carrier dynamics.[2] Besides heteroepitaxial strain, another possible cause for the induced polarity might be the one-dimensional geometry of the nanowires, which could enhance the effective internal field[22] and promote charge separation over longer lengths. To examine this, we performed the same measurements on heteroepitaxial surface-guided $CsPbBr_3$ square nanoplatelets on flat C-plane sapphire, which were synthesized in the same method as the nanowires (appear occasionally on the sample in between the nanowires). The

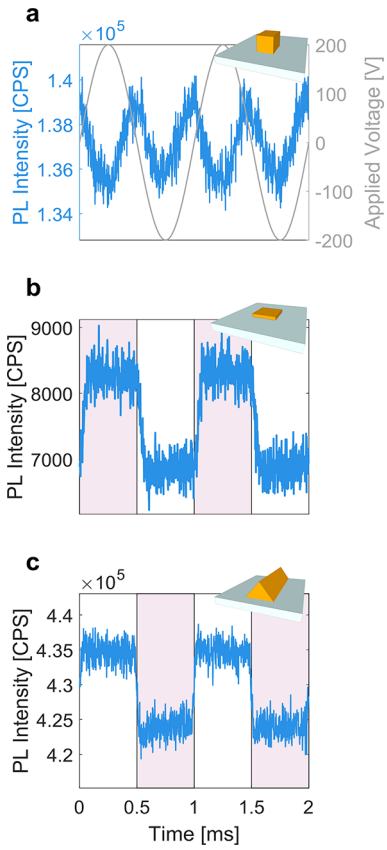

Figure 4. E-field-dependent PL intensity modulation of other $CsPbBr_3$ crystals. (a) Representative E-field-dependent PL modulation of solution-dispersed $CsPbBr_3$ crystals to a 200 V sine wave at 1 kHz (2% modulation depth). (b) Representative PL intensity modulation of heteroepitaxial $CsPbBr_3$ nanoplatelets grown on C-plane sapphire to an applied 10 V square wave at 1 kHz (15% modulation depth). (c) Representative PL intensity modulation of $CsPbBr_3$ nanowires grown on amorphous SiO_2 to an applied 10 V square wave at 1 kHz (3% modulation depth). In (b) and (c), the purple areas refer to 10 V and the white area refers to −10 V according to the lab frame. Insets: Schemes of the examined $CsPbBr_3$ crystal: (a) dispersed microcrystal, (b) surface-guided nanoplatelet on sapphire, and (c) nanowire grown on SiO_2.

nanoplatelets, ∼1 μm^2 in area and up to 200 nm in height, display an asymmetric response (Figure 4b) with a modulation depth of the same order of magnitude as the nanowires. This finding further establishes heteroepitaxial strain, and not geometry, as the main cause of the apparent internal dipole. Even nonepitaxial relations with an amorphous SiO_2 substrate cause an asymmetric response in horizontal nanowires, though with a much lower modulation depth (up to 3%, Figure 4c). In this case, since there are no epitaxial relations, the strain is introduced only upon cooling from synthesis- to room-temperature, due to the large difference between the thermal expansion coefficients of $CsPbBr_3$[24] and silica.[25] All these results seem to indicate a strain-related structural source for the significant asymmetric PL modulation.

Structural Investigation of Surface-Guided $CsPbBr_3$ Nanowires Using Low-Frequency Polarized Raman Spectroscopy. In order to complete the picture from a structural aspect, we used low-frequency polarized Raman spectroscopy to compare the structure of the heteroepitaxially strained nanowires before and after applying an external field. We illuminate the nanowires with a below-bandgap linearly

https://doi.org/10.1021/acsnano.1c04905
ACS Nano 2021, 15, 16130−16138

polarized laser (785 nm), then collect the scattered light using an analyzer in the parallel or perpendicular polarizations with respect to the incident beam (see Methods). We keep the sample orientation fixed, while the incoming light polarization is rotated every 10°, to obtain the Raman PO map. First, we examine the unpolarized Raman spectra, integrated over all polarizations (Figure 5a). It is immediately apparent that the

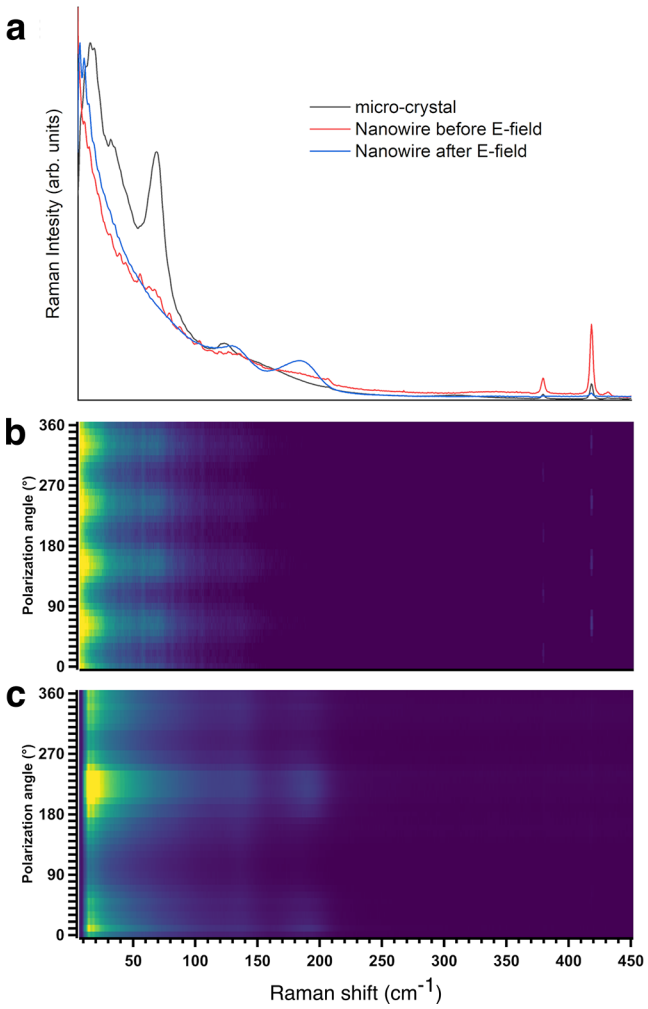

Figure 5. Polarized Raman spectroscopy of surface-guided $CsPbBr_3$ nanowires. (a) Normalized Raman spectra, integrated over all polarizations, of a microsized single crystal (black), a pristine surface-guided nanowire (red), and the same nanowire after applying an E-field (10 V square wave, 1 kHz, in blue). The sharp peaks at 379 and 418 cm^{-1} are characteristic of sapphire.[35] (b and c) Typical PO intensity maps of the same nanowire as in (a) at polarization orientation angles of 0−360° in perpendicular (⊥) polarization configuration (collection of the scattered light polarized perpendicularly to the laser excitation polarization), (b) is the pristine nanowire and, (c) is after applying an E-field. Each map is normalized independently; color scale is linear. All measurements were done in ambient conditions.

spectrum of the pristine nanowire is considerably more diffused than that of a single crystal, where the main observed signal is the central diffuse feature, or "central peak", indicative of relaxational atomic motion.[26,27] Additionally, the peaks at 75 and 128 cm^{-1} that are clearly visible in the bulk are only barely observed in the nanowire's spectrum. These predominant differences imply that the crystal structure of the nanowire is different than that of the bulk, likely due to strain.[2] Importantly, after applying an external E-field, the nanowire exhibits an additional flattening of the low-frequency peaks as well as a new broad peak at 188 cm^{-1}. This is in contrast with strain-free $CsPbBr_3$ crystals, which do not present distinguishable differences in the unpolarized Raman spectra before and after application of an external E-field (Figure S6c).

Further insight on the apparent differences between the nanowire before and after applying an E-field is gained when observing the complete PO maps. These color maps show the scattering intensity of the perpendicular configuration (parallel is shown in Figure S6) as a function of the incoming light polarization angle. The expected periodicity in the Raman signal of a single crystal is apparent in the nanowire before biasing (Figure 5b).[26] However, after applying an external AC field, the nanowire's PO Raman map (Figure 5c) shows loss of periodicity, which is indicative of an anisotropic structure, implying structural change on a mesoscopic level. Indeed, crystalline domains were reported before in single-crystal $CsPbBr_3$, attributed to a response of the perovskite's lattice to perturbations such as strain and temperature change.[28−30]

Our results imply that in the case of surface-guided nanowires, the combination of strain and the E-field could promote the creation of multiple crystalline domains with nonuniform crystallographic orientations, possibly as a means of minimizing the effect of the external forces.[31] This combination of strain and external E-field may reduce the energy required for breaking the ionic bonds, potentially increasing defect density and promoting formation of crystalline domains.[32] The existence of domains provides a possible explanation not only for the E-field-induced long-lasting polarization in the surface-guided $CsPbBr_3$ nanowires but also to the slow dynamics observed, as it may generate additional trap sites. This is further supported by the saturation of PL intensity modulation with increasing E-field (Figure 3d), which as mentioned above, indicates hindrance of spatial charge separation. In addition to the loss of periodicity in the PO maps, the appearance of a new Raman peak at 188 cm^{-1} further supports an occurrence of a structural change in the nanowires. This peak is not characteristic of the known $CsPbBr_3$ phases and its origin is yet to be determined.

In the case of $MAPbI_3$, the observation of polar domains was the most persuasive evidence for its ferroelectric behavior.[33] However, in $CsPbBr_3$, even though polar phases were reported before,[12,34] to the best of our knowledge, there is no established link between polar characteristics and crystalline domains. We note that second-harmonic generation (SHG) measurements performed on single nanowires showed no measurable SHG signal from the nanowires, neither before nor after applying an E-field, providing further evidence for the absence of a single polar domain in the nanowires. We propose two possible mechanisms of the dipole formation in the surface-guided nanowires upon formation of smaller crystalline domains: (1) The domain walls trap a high density of charge carriers due to an increased amount of defects, causing a long-lasting charge separation, observed as an internal dipole. (2) The domains constitute unit cells with a permanent polarity, and depending on the overall domains' orientation, a total polarization is produced. At this point, the exact dipole formation mechanism in the surface-guided $CsPbBr_3$ nanowires is unknown, as it is challenging to distinguish structural polarization from charge separation caused by interfacial effects and requires further evidence.

https://doi.org/10.1021/acsnano.1c04905
ACS Nano 2021, 15, 16130−16138

CONCLUSIONS

In conclusion, the PL of surface-guided heteroepitaxial $CsPbBr_3$ nanowires is strongly affected by external E-fields, allowing a switching of the emission of single nanowires with a modulation depth of up to 40%. This behavior is attributed to a combined effect of heteroepitaxial strain and an external E-field, giving rise to a permanent internal electrostatic field inside the nanowires, the direction of which could be set by the initial external field. PO Raman spectroscopy revealed the likely formation of crystalline domains in the nanowires under an external E-field, which led to the observed polarization. Furthermore, we have demonstrated how modulation of PL under an E-field can be used as a powerful tool to qualitatively assess the level of strain in an MHP system. These results shed light on the significant effect of an external E-field on the properties of strained MHPs, which can have a strong impact on the operation of MHP-based optoelectronics. In addition to the efficient charge separation these nanowires offer, which is highly beneficial for sensing and energy harvesting, their long excited-carrier storage on a millisecond time scale marks them as intriguing candidates for a variety of applications such as optically read memories and optical light modulators.

METHODS

Nanowire Synthesis. The surface-guided nanowires and nanoplatelets on sapphire and the nonepitaxial nanowires on amorphous SiO_2 were synthesized *via* two vapor-phase methods. For the first method, we used a spectroscopic hot plate (Linkam THMS600) with a round stage size of ∼2 cm radius, over which we placed chunks of molten CsBr+$PbBr_2$ powders (both 99.999%, purchased from Sigma-Aldrich). The sample is placed face down over an aluminum ring spacer, such that the distance from the chunks is ∼500 μm. The stage is then heated to 420 °C with a rate of 30 °C/min and kept at the nanowire growth temperature for 5−10 min, after which the stage is cooled to room temperature at a rate of ∼100 °C/min. For the second method, we use a similar approach, using a large hot plate instead.[7] In this method, the sample is not placed over the chunks upon heating, but is rather preheated for 1 min at the growth temperature. At the end of the synthesis the sample is rapidly cooled by removing it abruptly from the precursor chunks.

Electrode Fabrication. To evaporate electrodes over the surface-guided nanowires on sapphire, we used a custom-made shadow mask (Suron A.C.A LTD) consisting of an array of two-electrode devices with a nominal gap of 10 μm between the electrodes. The mask is made of stainless steel and is 0.5 mm in thickness. Before metal evaporation, the shadow mask was attached to the sapphire sample with alignment of the nanowires to the electrodes done under an optical microscope. The sample was taped to the shadow mask with Kapton tape, with an infrastructure of the same thickness sapphire frame, to minimize bending of the mask. We used an e-beam evaporator (Selene ODEM) to evaporate gold electrodes with a thickness of 150 nm, over a thin adhesive layer of chromium.

Electro-optic Setup. A 405 nm CW laser (OBIS, Coherent) was passed through a half-wave plate and a polarizer (Thorlabs, GT10-A), then coupled into an inverted microscope (Zeiss, Axiovert 200 inverted microscope) and was focused using an objective (Zeiss, Plan-Neofluar 20×/0.50 NA). The epi-detected signal passed through a dichroic mirror (Semrock, Di02-R488) and a band-pass filter (Semrock, BLP01-488R-25). The image was projected into one of three ports. One port was coupled into a spectrometer (Ocean Optics, USB4000) using a grating of 300 grooves/mm with 500 nm blaze wavelength. The second was projected into an EMCCD camera (Andor, iXon ultra) for orientation on the sample, and the third port was coupled into a multimode fiber (Thorlabs, FG050FGL) that is coupled to a SPAD (ID Quantique, ID100). The SPAD was connected to a TCSPC system (Picoquant HydraHarp 400). Triggers at 1 MHz were sent to the TCSPC using a function generator (Rigol, DG1022A) to mimic periodic excitation and to gain the precise time registration of single photons. All the measurements were done under ambient conditions.

The sapphire substrate with the guided nanowires and patterned with microelectrodes was placed on a glass slide in such a way that the nanowires were facing away from the microscope objective, allowing access of needles from above to create electric contact with any pair of deposited electrodes using probe positioners (Cascade Microtech, DPP-105-M-Al-S and Scientifica, Patch Star). In such conditions, the excitation beam passes through the glass and the sapphire substrate. The laser power in the experiment was approximately 3 μW, and the laser polarization was perpendicular to the nanowires' long axes. The PL signal was collected from a diffraction-limited spot approximately from the middle of the nanowire. The AC field was generated by a data acquisition (DAQ) card (National Instruments, PCI-6733) installed on the computer. A synchronized electronic signal (a marker) at the frequency of the AC is also sent to the TCSPC to mark the beginning of each voltage cycle, such that every photon arrival time can be referenced to the start of the AC wave. The AC wave and the markers were continuously monitored with an oscilloscope. The PL signal is then binned to 1000 bins between every 2 markers (in one period of the AC wave), meaning the bin size is ∼1 μs when a 1 kHz wave is applied. Over many AC cycles (measurement duration is ∼3 min), the histogram of the photon arrivals per time bin represents the photon emission behavior in accordance with the AC cycle.

Control Experiment Materials and Chemicals. The $CsPbBr_3$ microcrystals were synthesized *via* low-temperature solution growth by the method reported before in the literature.[23] The materials used were CsBr (99.9% trace metals basis, Sigma-Aldrich) and $PbBr_2$ (98%, Sigma-Aldrich), which were dissolved in dimethyl sulfoxide (DMSO, for HPLC, 99.7%, Sigma-Aldrich).

The colloidal $CsPbBr_3$ nanoparticles were synthesized in solution by the method reported before in the literature (10 nm[19] and 100 nm[36]). The chemicals used for preparation of the nanoparticles were Cs_2CO_3 (99.995%, Sigma-Aldrich), octadecene (ODE, 90%, Sigma-Aldrich), oleic acid (OA, 90%, Sigma-Aldrich), oleylamine (OLA, 70%, Sigma-Aldrich), $PbBr_2$ (98%, Sigma-Aldrich), toluene (99.8%, Sigma-Aldrich, anhydrous), hexane (99.5%, Sigma-Aldrich, anhydrous), and *N*,*N*-dimethylformamide (DMF, 99.8%, Sigma-Aldrich, anhydrous).

Polarization-Orientation Raman Spectroscopy. Raman measurements were performed with a custom-built system based on a 1000 mm focal length Horiba FHR-1000 dispersive spectrometer. Ultra-low-frequency Notch filters from ONDAX were used in the setup to allow access until the THz region (>10 cm^{-1}). Excitation from a Toptica diode laser tuned at 785 nm with a nominal power of 500 mW was used, and the broad spectrum of spontaneous emission was suppressed by four sequential ASE filters. The laser was focused on the sample by an optical microscope equipped with a 100× objective, which allows a nominal spatial resolution of about 1 μm. The combination of the 785 nm excitation line and the use of a holographic grating with 600 gr/mm coupled with a 1024 × 256 pixels CCD detector gave a maximum spectral resolution of ∼2 cm^{-1}.

The excitation at 785 nm had energy sufficiently low to avoid the photoluminescence, and the incoming power was reduced with a series of neutral density filters to prevent thermal effects even for longer acquisitions. The Raman polarization dependence of the nanowires before and after the exposure to the E-field was measured in parallel and perpendicular configurations with steps of 10° at 300 K. The incident light polarization angle of 0° was set to be aligned with the long axis of the nanowire. To control the polarization of the incident and scattered light, half-wave plates and a polarizer−analyzer combination were used as described in our previous work.[37]

Second-Harmonic Generation. Pulses of 100 fs at 1300 nm and at a repetition rate of 80 MHz were generated by a Coherent Chameleon Ultra II laser pumping an optical parametric oscillator. The beam passed through a GT10-C polarizer, a half-wave plate, and a liquid crystal (LC1113-C) into an inverted microscope (Zeiss, Axiovert 200, Zeiss objective: Plan-Neofluar 20×/0.50 NA) to control the incoming laser polarization and compensate for the polarization-

https://doi.org/10.1021/acsnano.1c04905
ACS Nano 2021, 15, 16130−16138

dependent phase of the dichroic mirror. The power density at the sample was 12 kW/m^2. The backscattered signal from the sample was filtered using a dichroic mirror (Thorlabs, DMSP950R), a short pass filter (Thorlabs 785SP), and a long-pass filter (EdgeBasic 594LP). The SHG signal passed through a polarizer into a multimode fiber and was detected by a single-photon avalanche photodiode (ID Quantique, ID100), which was connected to a TCSPC system (Picoquant HydraHarp 400), accompanied by triggers of the same input laser. Polarimetry was performed by measuring the SHG intensity from a point along the nanowire as a function of excitation polarization, for two orthogonal output polarizations. Spectra were taken using a Princeton Instruments SpectraPro 2300i.

ASSOCIATED CONTENT

Supporting Information

The Supporting Information is available free of charge at https://pubs.acs.org/doi/10.1021/acsnano.1c04905.

Compositional structure by energy dispersive X-ray spectroscopy of the surface-guided $CsPbBr_3$ nanowires, PL spectra in response to application of an E-field, E-field-dependent charge carrier dynamics model, investigating the origin of the linear PL intensity modulation, supplemental polarization-orientation Raman spectroscopy data (PDF)

AUTHOR INFORMATION

Corresponding Authors

Ernesto Joselevich − *Department of Molecular Chemistry and Materials Science, Weizmann Institute of Science, Rehovot 76100, Israel;* orcid.org/0000-0002-9919-0734; Email: dan.oron@weizmann.ac.il

Dan Oron − *Department of Molecular Chemistry and Materials Science, Weizmann Institute of Science, Rehovot 76100, Israel;* orcid.org/0000-0003-1582-8532; Email: ernesto.joselevich@weizmann.ac.il

Authors

Ella Sanders − *Department of Molecular Chemistry and Materials Science, Weizmann Institute of Science, Rehovot 76100, Israel*

Yahel Soffer − *Physics of Complex Systems, Weizmann Institute of Science, Rehovot 76100, Israel;* orcid.org/0000-0002-7082-6647

Tommaso Salzillo − *Chemical and Biological Physics, Weizmann Institute of Science, Rehovot 76100, Israel*

Maor Rosenberg − *Physics of Complex Systems, Weizmann Institute of Science, Rehovot 76100, Israel*

Omri Bar-Elli − *Physics of Complex Systems, Weizmann Institute of Science, Rehovot 76100, Israel*

Omer Yaffe − *Chemical and Biological Physics, Weizmann Institute of Science, Rehovot 76100, Israel;* orcid.org/0000-0003-4114-7968

Complete contact information is available at: https://pubs.acs.org/10.1021/acsnano.1c04905

Author Contributions

#E.S. and Y.S. contributed equally to this work.

Notes

The authors declare no competing financial interest.

ACKNOWLEDGMENTS

The authors thank Dr. Ron Tenne, Dr. Venkata Jayasurya Yallapragada, Dr. Regev Ben Zvi, Dr. David Ehre, Prof. Aron Walsh, and Prof. David Cahen for fruitful discussions, and Dekel Nakar for critically reviewing the manuscript. We are grateful to Dr. Miri Kazes and Dr. Gili Yaniv for providing the colloidal $CsPbBr_3$ QDs samples, their TEM images, and analysis and for sharing their useful MHP structural insights. We thank Dr. Sigalit Aharon for providing the $CsPbBr_3$ microcrystals. E.S. is supported by the Sustainability and Energy Research Initiative (SAERI) at the Weizmann Institute. Y.S. is supported by the Ariane de Rothschild Women Doctoral Program. D.O. is the incumbent of the Harry Weinrebe Professorial Chair of laser physics. E.J. is the incumbent of the Drake Family Professorial Chair of Nanotechnology and Director of the Helen and Martin Kimmel Centre for Nanoscale Science at the Weizmann Institute.

REFERENCES

(1) Moloney, E. G.; Yeddu, V.; Saidaminov, M. I. Strain Engineering in Halide Perovskites. *ACS Mater. Lett.* **2020**, *2*, 1495−1508.

(2) Chen, Y.; Lei, Y.; Li, Y.; Yu, Y.; Cai, J.; Chiu, M.-H.; Rao, R.; Gu, Y.; Wang, C.; Choi, W.; Hu, H.; Wang, C.; Li, Y.; Song, J.; Zhang, J.; Qi, B.; Lin, M.; Zhang, Z.; Islam, A. E.; Maruyama, B.; et al. Strain Engineering and Epitaxial Stabilization of Halide Perovskites. *Nature* **2020**, *577*, 209−215.

(3) Tsai, H.; Asadpour, R.; Blancon, J.-C.; Stoumpos, C. C.; Durand, O.; Strzalka, J. W.; Chen, B.; Verduzco, R.; Ajayan, P. M.; Tretiak, S.; Even, J.; Alam, M. A.; Kanatzidis, M. G.; Nie, W.; Mohite, A. D. Light-Induced Lattice Expansion Leads to High-Efficiency Perovskite Solar Cells. *Science* **2018**, *360*, 67−70.

(4) Sharma, M.; Kumar, A.; Ahluwalia, P.; Pandey, R. Strain and Electric Field Induced Electronic Properties of Two-Dimensional Hybrid Bilayers of Transition-Metal Dichalcogenides. *J. Appl. Phys.* **2014**, *116*, 063711.

(5) Oksenberg, E.; Sanders, E.; Popovitz-Biro, R.; Houben, L.; Joselevich, E. Surface-Guided $CsPbBr_3$ Perovskite Nanowires on Flat and Faceted Sapphire with Size-Dependent Photoluminescence and Fast Photoconductive Response. *Nano Lett.* **2018**, *18*, 424−433.

(6) Oksenberg, E.; Merdasa, A.; Houben, L.; Kaplan-Ashiri, I.; Rothman, A.; Scheblykin, I. G.; Unger, E. L.; Joselevich, E. Large Lattice Distortions and Size-Dependent Bandgap Modulation in Epitaxial Halide Perovskite Nanowires. *Nat. Commun.* **2020**, *11*, 1−11.

(7) Wang, Y.; Yasar, M.; Luo, Z.; Zhou, S.; Yu, Y.; Li, H.; Yang, R.; Wang, X.; Pan, A.; Gan, L. Temperature Difference Triggering Controlled Growth of All-Inorganic Perovskite Nanowire Arrays in Air. *Small* **2018**, *14*, 1803010.

(8) Oksenberg, E.; Popovitz-Biro, R.; Rechav, K.; Joselevich, E. Guided Growth of Horizontal ZnSe Nanowires and Their Integration into High-Performance Blue−UV Photodetectors. *Adv. Mater.* **2015**, *27*, 3999−4005.

(9) Shalev, E.; Oksenberg, E.; Rechav, K.; Popovitz-Biro, R.; Joselevich, E. Guided CdSe Nanowires Parallelly Integrated into Fast Visible-Range Photodetectors. *ACS Nano* **2017**, *11*, 213−220.

(10) Tsivion, D.; Schvartzman, M.; Popovitz-Biro, R.; von Huth, P.; Joselevich, E. Guided Growth of Millimeter-Long Horizontal Nanowires with Controlled Orientations. *Science* **2011**, *333*, 1003−1007.

(11) Park, K.; Deutsch, Z.; Li, J. J.; Oron, D.; Weiss, S. Single Molecule Quantum-Confined Stark Effect Measurements of Semiconductor Nanoparticles at Room Temperature. *ACS Nano* **2012**, *6*, 10013−10023.

(12) Li, X.; Chen, S.; Liu, P.-F.; Zhang, Y.; Chen, Y.; Wang, H.-L.; Yuan, H.; Feng, S. Evidence for Ferroelectricity of All-Inorganic Perovskite $CsPbBr_3$ Quantum Dots. *J. Am. Chem. Soc.* **2020**, *142*, 3316−3320.

(13) Lehmann, A. G.; Congiu, F.; Marongiu, D.; Mura, A.; Filippetti, A.; Mattoni, A.; Saba, M.; Pegna, G.; Sarritzu, V.; Quochi, F. Long-

Lived Electrets and Lack of Ferroelectricity in Methylammonium Lead Bromide $CH_3NH_3PbBr_3$ Ferroelastic Single Crystals. *Phys. Chem. Chem. Phys.* **2021**, *23*, 3233−3245.
(14) Kao, K. C. *Electrets. Dielectric Phenomena in Solids*; Elsevier: San Diego, 2004; pp 283−326.
(15) Qiu, C.; Grey, J. K. Modulating Charge Recombination and Structural Dynamics in Isolated Organometal Halide Perovskite Crystals by External Electric Fields. *J. Phys. Chem. Lett.* **2015**, *6*, 4560−4565.
(16) Sharma, D. K.; Hirata, S.; Biju, V.; Vacha, M. Stark Effect and Environment-Induced Modulation of Emission in Single Halide Perovskite Nanocrystals. *ACS Nano* **2019**, *13*, 624−632.
(17) Wang, Z.; Huang, Z.; Liu, G.; Cai, B.; Zhang, S.; Wang, Y. *In Situ* and Reversible Enhancement of Photoluminescence from $CsPbBr_3$ Nanoplatelets by Electrical Bias. *Adv. Opt. Mater.* **2021**, *9*, 2100346.
(18) Sewvandi, G. A.; Hu, D.; Chen, C.; Ma, H.; Kusunose, T.; Tanaka, Y.; Nakanishi, S.; Feng, Q. Antiferroelectric-to-Ferroelectric Switching in $CH_3NH_3PbI_3$ Perovskite and Its Potential Role in Effective Charge Separation in Perovskite Solar Cells. *Phys. Rev. Appl.* **2016**, *6*, 024007.
(19) Protesescu, L.; Yakunin, S.; Bodnarchuk, M. I.; Krieg, F.; Caputo, R.; Hendon, C. H.; Yang, R. X.; Walsh, A.; Kovalenko, M. V. Nanocrystals of Cesium Lead Halide Perovskites ($CsPbX_3$, X= Cl, Br, and I): Novel Optoelectronic Materials Showing Bright Emission with Wide Color Gamut. *Nano Lett.* **2015**, *15*, 3692−3696.
(20) Oksenberg, E.; Fai, C.; Scheblykin, I. G.; Joselevich, E.; Unger, E. L.; Unold, T.; Hages, C.; Merdasa, A. Deconvoluting Energy Transport Mechanisms in Metal Halide Perovskites Using $CsPbBr_3$ Nanowires as a Model System. *Adv. Funct. Mater.* **2021**, *2021*, 2010704.
(21) Kraus, R.; Lagoudakis, P.; Rogach, A.; Talapin, D.; Weller, H.; Lupton, J.; Feldmann, J. Room-Temperature Exciton Storage in Elongated Semiconductor Nanocrystals. *Phys. Rev. Lett.* **2007**, *98*, 017401.
(22) Rothenberg, E.; Kazes, M.; Shaviv, E.; Banin, U. Electric Field Induced Switching of the Fluorescence of Single Semiconductor Quantum Rods. *Nano Lett.* **2005**, *5*, 1581−1586.
(23) Rakita, Y.; Kedem, N.; Gupta, S.; Sadhanala, A.; Kalchenko, V.; Böhm, M. L.; Kulbak, M.; Friend, R. H.; Cahen, D.; Hodes, G. Low-Temperature Solution-Grown $CsPbBr_3$ Single Crystals and Their Characterization. *Cryst. Growth Des.* **2016**, *16*, 5717−5725.
(24) Stoumpos, C. C.; Malliakas, C. D.; Peters, J. A.; Liu, Z.; Sebastian, M.; Im, J.; Chasapis, T. C.; Wibowo, A. C.; Chung, D. Y.; Freeman, A. J. Crystal Growth of the Perovskite Semiconductor $CsPbBr_3$: A New Material for High-Energy Radiation Detection. *Cryst. Growth Des.* **2013**, *13*, 2722−2727.
(25) Vlugter, P.; Block, E.; Bellouard, Y. Local Tuning of Fused Silica Thermal Expansion Coefficient Using Femtosecond Laser. *Phys. Rev. Mater.* **2019**, *3*, 053802.
(26) Yaffe, O.; Guo, Y.; Tan, L. Z.; Egger, D. A.; Hull, T.; Stoumpos, C. C.; Zheng, F.; Heinz, T. F.; Kronik, L.; Kanatzidis, M. G. Local Polar Fluctuations in Lead Halide Perovskite Crystals. *Phys. Rev. Lett.* **2017**, *118*, 136001.
(27) Sharma, R.; Dai, Z.; Gao, L.; Brenner, T. M.; Yadgarov, L.; Zhang, J.; Rakita, Y.; Korobko, R.; Rappe, A. M.; Yaffe, O. Elucidating the Atomistic Origin of Anharmonicity in Tetragonal $CH_3NH_3PbI_3$ with Raman Scattering. *Phys. Rev. Mater.* **2020**, *4*, 092401.
(28) Li, X.; Luo, Y.; Holt, M. V.; Cai, Z.; Fenning, D. P. Residual Nanoscale Strain in Cesium Lead Bromide Perovskite Reduces Stability and Shifts Local Luminescence. *Chem. Mater.* **2019**, *31*, 2778−2785.
(29) Bertolotti, F.; Protesescu, L.; Kovalenko, M. V.; Yakunin, S.; Cervellino, A.; Billinge, S. J. L.; Terban, M. W.; Pedersen, J. S.; Masciocchi, N.; Guagliardi, A. Coherent Nanotwins and Dynamic Disorder in Cesium Lead Halide Perovskite Nanocrystals. *ACS Nano* **2017**, *11*, 3819−3831.
(30) Marçal, L. A.; Oksenberg, E.; Dzhigaev, D.; Hammarberg, S.; Rothman, A.; Björling, A.; Unger, E.; Mikkelsen, A.; Joselevich, E.; Wallentin, J. *In Situ* Imaging of Ferroelastic Domain Dynamics in $CsPbBr_3$ Perovskite Nanowires by Nanofocused Scanning X-Ray Diffraction. *ACS Nano* **2020**, *14*, 15973−15982.
(31) Arlt, G. Twinning in Ferroelectric and Ferroelastic Ceramics: Stress Relief. *J. Mater. Sci.* **1990**, *25*, 2655−2666.
(32) Wilson, J. N.; Frost, J. M.; Wallace, S. K.; Walsh, A. Dielectric and Ferroic Properties of Metal Halide Perovskites. *APL Mater.* **2019**, *7*, 010901.
(33) Rakita, Y.; Bar-Elli, O.; Meirzadeh, E.; Kaslasi, H.; Peleg, Y.; Hodes, G.; Lubomirsky, I.; Oron, D.; Ehre, D.; Cahen, D. Tetragonal $CH_3NH_3PbI_3$ Is Ferroelectric. *Proc. Natl. Acad. Sci. U. S. A.* **2017**, *114*, E5504−E5512.
(34) Gao, X.; Wang, Q.; Zhang, Y.; Cui, C.; Sui, N.; Chi, X.; Zhang, H.; Zhou, Q.; Bao, Y.; Wang, Y. Pressure Effects on Optoelectronic Properties of $CsPbBr_3$ Nanocrystals. *J. Phys. Chem. C* **2020**, *124*, 11239−11247.
(35) Thapa, J.; Liu, B.; Woodruff, S. D.; Chorpening, B. T.; Buric, M. P. Raman Scattering in Single-Crystal Sapphire at Elevated Temperatures. *Appl. Opt.* **2017**, *56*, 8598−8606.
(36) Cao, Y.; Zhu, W.; Li, L.; Zhang, Z.; Chen, Z.; Lin, Y.; Zhu, J.-J. Size-Selected and Surface-Passivated $CsPbBr_3$ Perovskite Nanocrystals for Self-Enhanced Electrochemiluminescence in Aqueous Media. *Nanoscale* **2020**, *12*, 7321−7329.
(37) Asher, M.; Angerer, D.; Korobko, R.; Diskin-Posner, Y.; Egger, D. A.; Yaffe, O. Anharmonic Lattice Vibrations in Small-Molecule Organic Semiconductors. *Adv. Mater.* **2020**, *32*, 1908028.

https://doi.org/10.1021/acsnano.1c04905
ACS Nano 2021, 15, 16130−16138